

pubs.acs.org/JPCB Article

# Penetration of Cell Surface Glycocalyx by Enveloped Viruses Is Aided by Weak Multivalent Adhesive Interaction

Xinyu Cui, X. Frank Zhang, and Anand Jagota\*



Cite This: J. Phys. Chem. B 2023, 127, 486-494



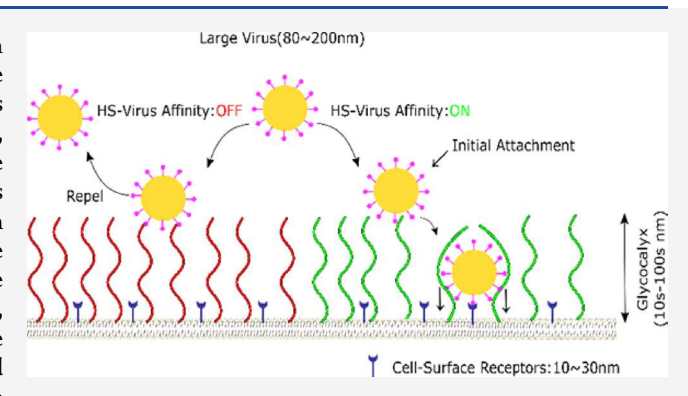
**ACCESS** I

Metrics & More

Article Recommendations

Supporting Information

ABSTRACT: Viral infection usually begins with adhesion between the viral particle and viral receptors displayed on the cell membrane. The exterior surface of the cell membrane is typically coated with a brush-like layer of molecules, the glycocalyx, that the viruses need to penetrate. Although there is extensive literature on the biomechanics of virus—cell adhesion, much of it is based on continuum-level models that do not address the question of how virus/cell-membrane adhesion occurs through the glycocalyx. In this work, we present a simulation study of the penetration mechanism. Using a coarse-grained molecular model, we study the force-driven and diffusive penetration of a brush-like glycocalyx by viral particles. For force-driven penetration, we find that viral particles smaller than the spacing of molecules in the



brush reach the membrane surface readily. For a given maximum force, viral particles larger than the minimum spacing of brush molecules arrest at some distance from the membrane, governed by the balance of elastic and applied forces. For the diffusive case, we find that weak but multivalent attraction between the glycocalyx molecules and the virus effectively leads to its engulfment by the glycocalyx. Our finding provides potential guidance for developing glycocalyx-targeting drugs and therapies by understanding how virus—cell adhesion works.

## INTRODUCTION

The emergence of many viral-related diseases poses a continuous risk to human health and has caused major viral outbreaks and pandemics over the past few decades. For example, the Ebola virus, which causes a deadly disease, was first discovered in 1976 and has caused more than 15,000 deaths. Middle East Respiratory Syndrome, first identified in 2012, is a viral respiratory illness primarily found in countries of the Middle East. The virus that causes the disease is one of the common coronaviruses. The current pandemic is caused by the emergence of a novel severe acute respiratory syndrome coronavirus 2, which has spread rapidly worldwide with serious harm to human health and our economy. This virus will likely be of ongoing concern due to its mutability. Consequently, understanding how virus particles infect human cells is important for developing vaccines and therapies.

Viruses can be classified into two major types based on their structure: enveloped or non-enveloped. Ebola, MERS, and SARS-Cov-2 belong to the former group in that they have a lipid layer covering capsids, the protein shells that enclose the viral genome. The adhesion of these viruses to the cell membrane is by binding between ligands displayed on the viral surface and receptors on the host cell membrane. They are subsequently engulfed through endocytosis or a similar process and eventually fuse their outer layer with host cell's membrane-

bound organelles (e.g., endosomes).<sup>11–13</sup> Clearly, the initial adhesion between the virus and cell membrane receptors is a critical event and understanding it is important.

The host cell membrane of eukaryotic cells often displays a brush-like complex layer on its outer surface named the glycocalyx. <sup>14</sup> The main components of the glycocalyx are proteoglycans, glycolipids, glycoproteins, and proteins, <sup>15</sup> of which the proteoglycans are generally considered to function as the essential molecules. <sup>16</sup> Proteoglycans are composed of a core protein to which one or more glycosaminoglycan (GAG) chains are attached. <sup>16</sup>

The GAG chains are linear polymers with varied lengths of disaccharides that are sulfated and/or acetylated to some extent. Each disaccharide consists of uronic acid and hexosamine. Depending on which uronic acid or hexosamine is integrated, the GAG chains can be categorized into five types: heparan sulfate (HS), 17 chondroitin sulfate, dermatan sulfate, keratan sulfate, and hyaluronic acid (or hyaluronan). 16

Received: September 19, 2022 Revised: December 17, 2022 Published: January 4, 2023





In the vasculature, HS is the most common GAG. <sup>15,18,19</sup> The HS chain consists of 50–150 units of disaccharides, resulting in a 50–150 nm contour length. <sup>20,21</sup> The HS proteoglycans are globally negatively charged and can bind to positively charged ions and plasma proteins or repel negatively charged molecules through electrostatic repulsion. <sup>16,22</sup>

For a long time, the glycocalyx has been regarded as a physical barrier regulating both pathogen adhesion and endothelial permeability due to its dense brush-like structure. The virus must penetrate this protective layer to adhere to a receptor on the host cell membrane. However, the height of the glycocalyx is typically significantly higher than that of the membrane-bound receptors, which raises a fundamental question: Given that such a shield exists on the surface of all eukaryotic cells, how does the virus make contact with receptors on the cell?

The main focus of the work we report here is to address this question, in which we examine three related hypotheses (Figure 1):

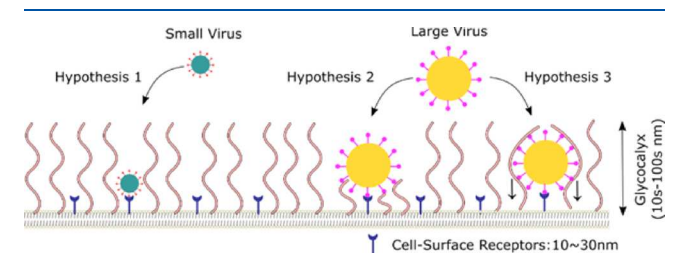


Figure 1. Three hypotheses to explain how the virus penetrates the glycocalyx: (1) small viruses can readily penetrate via the gaps between glycocalyx constituents. (2) Large viruses can bend and squeeze the soft glycocalyx under external load until they find the receptor. (3) Large viruses can use their weak but multivalent affinity with HS to be engulfed by and diffuse in the glycocalyx layer.

- 1. If the virus is small enough compared to the gaps between glycocalyx constituents, it can penetrate easily.
- If the virus is larger than the characteristic distance between chains, with the aid of external forces, it can bend and squeeze the soft glycocalyx until it finds the receptor.
- The virus may utilize its weak but multivalent attractive interaction with HS to be engulfed into and diffuse within the glycocalyx.

To examine these hypotheses, we developed a coarsegrained simulation model for the system, as described in detail later. A critical choice is deciding on the representation of the glycocalyx. Depending on the level of detail, most glycocalyx models fall into one of three categories. In increasing level of complexity, these are at the (a) continuum, (b) coarse-grained (CG) model, or (c) all-atom level. In continuum models, the glycocalyx has been described as a single-layer elastic material, double-layer structure, and brush-like polymer layer, while modeling interaction with the virus using Hertz contact mechanics or polymer brush physics. <sup>23–28</sup> While continuum models provide much insight, they are not suited to investigate our hypotheses because of the difficulty of incorporating key elements such as a discrete structure through which a viral particle can move, negatively charged flexible chains, thermal fluctuations, and control over interactions such as the virusreceptor interaction potential in this complex glycocalyx structure. Large-scale, all-atom molecular models, simulated

using molecular dynamics, capture much more of the detail and are, hence, more realistic. <sup>29,30</sup> However, because of their detailed nature, they apply only to particular systems and are not the most desirable when one is interested in extracting more general results and understanding. We chose instead to develop a coarse-grained model, which has some advantages over the other two because (a) compared to the continuum models, it can at the same time represent continuum properties as well as a discrete structure, e.g., allowing engulfment and penetration, and (b) compared to all-atom models, it requires relatively modest computational power and can provide more general results by simplification and idealization.

In the remainder of this manuscript, we first describe the construction of the coarse-grained model, including the glycocalyx, host cell receptors, and virion. We then describe and discuss the results of Brownian dynamics simulations using the CG model that address our hypotheses.

## METHODS

We wish to create a generic CG model including a viral particle, the glycocalyx, and receptors. We constructed a CG model for the glycocalyx by focusing on its main component, HS chains. These are represented as chains of beads arranged as a brush-like array with one end attached to an immobile surface representing the cell membrane. Multiple potentials were applied in the system as summarized in Table 1.

The system comprised a chain of HS beads, virus beads, and receptor chains consisting of one virus-binding bead and multiple backbone beads. The HS was represented by a string of connected beads; a single bead representing a monomer of the HS chain, with size and charge of  $D_{\rm HS}=1~{\rm nm}^{19}$  and  $q=-3.2~\times~10^{-19}{\rm C.}^{31}$  Adjacent HS beads on a chain were connected by stiff spring potentials and bending potentials for each set of three adjacent beads. The spring constant  $K_s$  for the spring potentials was set at a sufficiently high value (100 N/m) to constrain the inter-bead distance to remain approximately at its natural length,  $r_0$ . The bending constant  $k_\theta$  was chosen to match the HS's known persistence length.  $^{30,32}$ 

$$E_{\theta} = k_{\theta}(\theta - \theta_0)^2 \tag{1}$$

where  $E_{\theta}$  is the harmonic angle energy,  $k_{\theta}$  is the bending constant,  $\theta$  is the harmonic angle, and  $\theta_0$  is the equilibrium value of the angle. The bending constant  $k_{\theta}$  is related to the persistence length,  $l_{p}$ , through the following expression:<sup>33</sup>

$$k_{\theta} = \frac{l_{\rm p}k_{\rm B}T}{l} \tag{2}$$

where  $k_{\rm B}$  is the Boltzmann constant, T is the absolute temperature, and l is the contour length of a chain of three connected beads. Syndecans were chosen as the core proteins for the HS proteoglycans as they are one of the most common and essential components of the glycocalyx. Since they are membrane-bound proteins, they were implicitly represented in the model by immobilizing one end of each HS chain onto the cell membrane.

For the representation of viruses, we used a generic spherical bead with a diameter in the range 10–200 nm, which spans the size of many significant viruses such as Hepatitis A virus (30 nm in diameter), Human Immunodeficiency Virus (approximately 100 nm in diameter), and SARS-CoV-2 (70–110 nm in diameter). We chose to build the host–cell receptors in two parts: (a) a binding domain, and (b) a flexible backbone,

Table 1. Coarse-Grained Model Parameters

	Heparan Sulfate		
Bead type	Diameter (nm)	Charge (C)	
Heparan Sulfate (HS)beads	1	-3.20E-19	
Harmonic bond	$E_{spring} = k_s(r - r_0)^2$		
Between	$k_s^{ m (N/m)}$	$r_0^{(\mathrm{nm})}$	
IS-HS	100	1	
Harmonic angle	$E_{\theta} = k_{\theta}$	$(\theta - \theta_0)^2$	
Between	$k_{ heta}^{ ext{(J/rad2)}}$	$ heta_0^{ ext{(rad)}}$	
IS-HS-HS	2.06E-20 J	$\pi$	
HS Density/Spacing			
Distance between adjacent HS chain an-			
chors	20 to	80 nm	
	Virus		
sead type	Diameter (nm)	Charge (C)	
Virus	10-200nm	0	
H	lost Cell receptors		
Bead type	Diameter (nm)	Charge (C)	
eceptor beads	6	1.60E-19	
Glycoproteins beads	1	-3.20E-19	
Harmonic bond			
Between	(N/m)	(nm)	
Receptor-Glycoprotein	100	3.5	
llycoprotein	100	1	
Harmonic angle			
Between	(J/rad2)	(rad)	

Po	ten	tia	ls

2.06E-21

 $\pi$ 

 $\pi$ 

Receptor-Glycoprotein-Glycoprotein

Glycoprotein-Glycoprotein-Glycoprotein

Cell Membrane Repulsion	$F = -F_0 exp\left(-\frac{Z - Z_0}{L}\right)$				
$F_0$ (nN)		$Z_0^{(nm)}$		L (nm)	
1		1		0.05	
Steric repulsion		$E = A \exp\left(\frac{\sigma - r}{\rho}\right) - \frac{C}{r^6} + \frac{D}{r^8}$			
Туре	A(J)	$\sigma^{(\mathrm{m})}$	$ ho^{\mathrm{(m)}}$	C (J*m6)	D(J*m8)
	6.00E-	1.00E-			
Between HS-HS	21	09	4.00E-10	0	0
	6.00E-	8.00E-			
Between Virus-Virus	21	08	4.00E-10	0	0
	6.00E-	4.05E-			
Between Virus-HS	21	08	4.00E-10	0	0
Between Receptor-Glyco-	6.00E-	2.50E-			
proteins	21	09	4.00E-10	0	0
Between Glycoproteins-Gly-	6.00E-	1.00E-			
coproteins	21	09	4.00E-10	0	0

Adhesive Poten	tials		$E = A \exp\left(-\frac{1}{2}\right)$	$\left(\frac{\sigma-r}{\rho}\right)-\frac{C}{r^6}$	$+\frac{D}{r^8}$
Type	A (J)	$\sigma^{\rm (m)}$	$\rho^{(m)}$	C (J*m6)	D(J*m8)
	1.65E-	5.30E-			
Between Receptor-Virus	18	08	5.10E-09	9.00E-62	0
	8.25E-	5.20E-			
Between HS-Virus (0.5KbT)	21	08	5.10E-09	4.50E-64	0
	1.65E-	5.20E-			
Between HS-Virus(1KbT)	20	08	5.10E-09	9.00E-64	0
	3.30E-	5.20E-			
Between HS-Virus(2KbT)	20	08	5.10E-09	1.80E-63	0
	6.60E-	5.20E-			

which is similar to the TIM family of receptors that the Ebola virus targets. Sizes of both receptor and backbone beads were chosen based on typical actual values. 35,36 One end of each receptor chain was immobilized at the membrane surface. This represents a variety of receptors, e.g., TIM for Ebola and Angiotensin-Converting Enzyme 2 for SARS-CoV-2. 36,37

pubs.acs.org/JPCB

The adhesive interaction between the virus and cell receptors was simulated as in our previous work<sup>17</sup> through the Born-Mayer-Huggins or Tosi/Fumi potentials implemented in the molecular modeling package, LAMMPS<sup>38</sup> (Table 1). The attractive potential well-depth was chosen based on the binding free energy of the Ebola virus<sup>39,40</sup> and SARS-CoV-2.41 The steric hindrance between every pair of beads in the system was also simulated by the same potential expression above but lacking the adhesion term; the corresponding distance between bead centers was the sum of individual bead radii for both adhesive and steric interactions; see Table 1 for details.

At the bottom of the system was the cell membrane, which we represented by a plane with a short-range (~1 nm) repulsion to make it impenetrable by any of the beads. 42 The pre-factor of the expression,  $F_0$ , was set as 1 nN to provide sufficient resistance to prevent any other bead in the system from penetrating through the membrane plane. We did not include any explicit water particles or ions; these were implicit in the model through our use of Langevin dynamics and screened Coulombic potentials (Table 1) to simulate their molecular friction, random thermal forces, and screened electrostatics.

This model was implemented in LAMMPS, and the problem was solved through Brownian dynamics using Langevin Dynamics methods. The first important step to construct the coarse-grained model of the HS chain was randomization of a single chain, so that one may pick a conformation from an equilibrium ensemble. This was achieved in three stages (Figure 2). (1) Heating: the HS chain was heated from 298.15

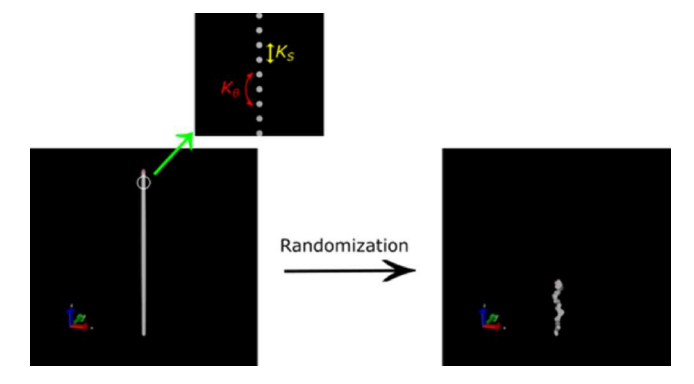


Figure 2. Randomization process for a single, approximately inextensible, HS chain. The single chain underwent a cycle of heating and cooling: 298.15-5000 K in 200 ns; 5000 K back to 298.15 K in 200 ns; holding at 298.15 K for an additional 400 ns.

to 5000 K in 200 ns. (2) Cooling: the chain was cooled from 5000 K back to 298.15 in 200 ns.(3) Hold: the system was held at 298.15 K for an additional 400 ns to confirm it was in equilibrium and to obtain snapshots from the equilibrium ensemble. Additional simulation details and methods for single-chain equilibrium verification are described in the SI section (S1). (The high temperature employed in the process is only to accelerate the randomization process.) The results

were analyzed using scripts written in MATLAB and visual molecular dynamics.  $^{43}$ 

We used the so-obtained ensemble of single randomized HS chains to build CG models of the brush by attaching single chains vertically with one end fixed onto the membrane plane. Brush density was adjusted by varying the spacing between chains between 20 and 80 nm. <sup>44</sup> It is worth noting that the elasticity of the brush is primarily entropic in nature and this is captured automatically by the simulation.

## RESULTS AND DISCUSSION

Effect of Virus Size and External Force. To examine the first and second hypotheses, we conducted a series of simulations of partial glycocalyx indentation (compression) by viral particles in which the virus bead was pushed onto the glycocalyx at a constant rate of 10 pN/ns for 2 ns. Figure 3

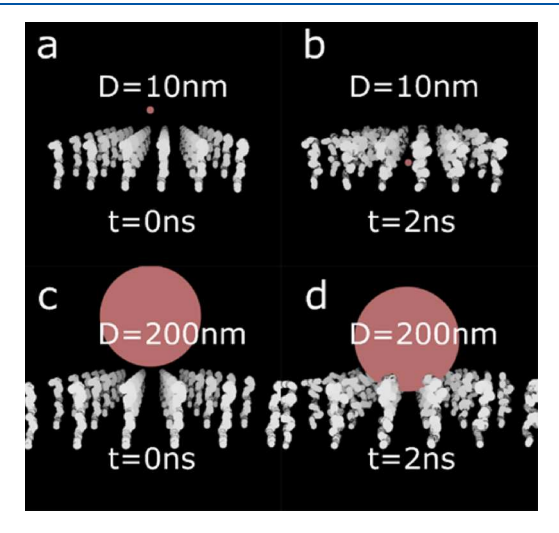
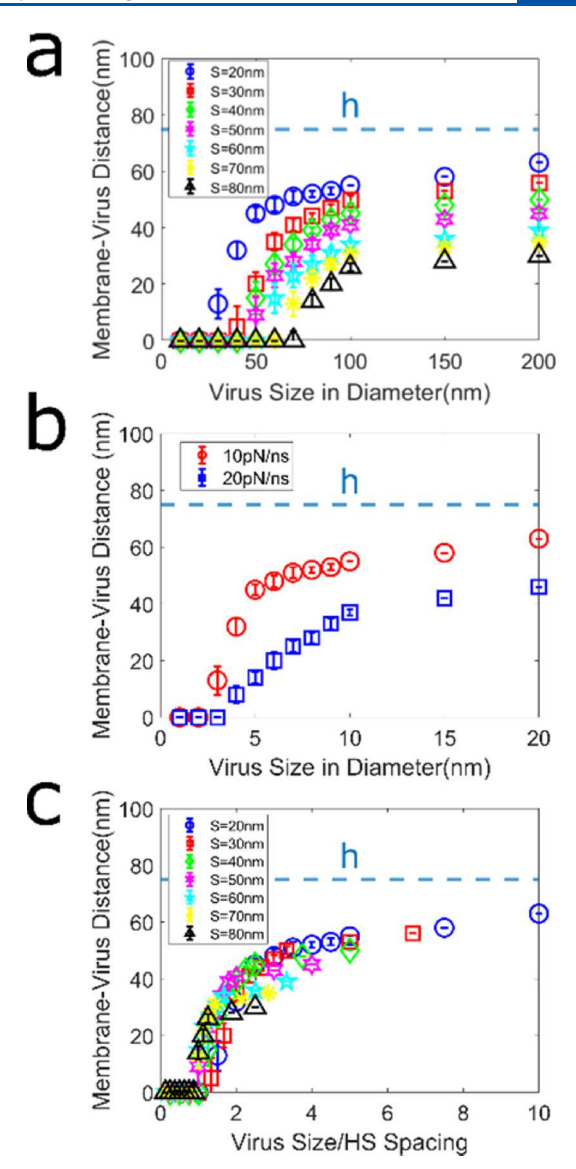


Figure 3. Snapshots from different stages of a typical indentation for small (a,b) and large viruses (c,d).

shows four snapshots from typical indentation simulations for both the small ( $D=10~\mathrm{nm}$ ) and large virus ( $D=200~\mathrm{nm}$ ) cases. The result shows that small viruses can readily be pushed through the gap between HS chains with the aid of external force while the large virus particles are arrested some distance away from the cell membrane.

In Figure 4a, we plot the indentation depth as a function of virus size for varying HS density. In addition to the observation in Figure 3, Figure 4a shows clearly that small viruses can easily penetrate the gap between HS chains with the aid of indentation force. However, once their size exceeds the gap between HS chains, the particles are arrested at some distance from the membrane by the glycocalyx, presumably by a balance of external force by elastic forces in the glycocalyx. Larger viruses arrest at smaller indentation depth because the elastic resistance they experience is larger. Figure 4b shows results for viruses with different diameters for spacing (S) = 20 nm and the same total time but two different loading rates showing that the arrest distance from the cell membrane for viruses larger than the gap depends on the total load applied. Thus, we conclude that (a) for the virus to get through the brush under external force, the critical question is whether it is larger or smaller than the gap between molecules; (b) if the virus size is smaller than the gap between HS chains, it goes easily and quickly to the membrane; and (c) if the virus size is larger than



**Figure 4.** In all figures, h refers to the undeformed height of the glycocalyx. (a) Plot of indentation depth as a function of virus size and HS density. Small viruses (compared to HS chain spacing) penetrate the glycocalyx structure and reach the membrane plane, while viruses larger than the spacing of the HS chain are arrested at some distance from the membrane. (b) Plot of indentation depth as a function of virus size for the case S=20 nm with two loading rates. A higher loading rate results in greater indentation because it reaches a higher load. Error bars show standard deviation. (c) Plot of indentation depth as a function of the ratio of virus size with HS mesh size. The same ratio with different virus and HS densities results in similar indentation depth.

the gap, the virus reaches a certain distance from the membrane depending on the maximum load applied. With sufficient force, it will reach the membrane.

In Figure 4c, we plot the indentation depth of the virus versus the ratio of virus size and HS spacing. Figure 4c shows that the indentation depth depends mainly on this ratio. Its critical value is 1, which decides whether a combination of virus size and HS mesh will allow the virus to pass through.

To understand these results, we propose a simple contact-mechanics model based on treating the HS brush as a Winkler Foundation.  $^{45-47}$ 

Consider the brush as a Winkler foundation under stress  $\sigma$ , of height h and constant k related to Young's modulus E (the detailed calculation of Young's modulus of the glycocalyx can be found in the SI, Section S2). For a Winkler foundation, stress  $\sigma$  is

$$\sigma = k\delta = E\frac{\delta}{h} \tag{3}$$

$$k = \frac{E}{h} \tag{4}$$

Let there be a gap in the foundation of diameter 2s, corresponding to the size into which the indenter can go without hindrance. Let us indent the Winkler foundation by  $\delta_0$  using a rigid sphere of radius R (Figure 5a). Although we draw

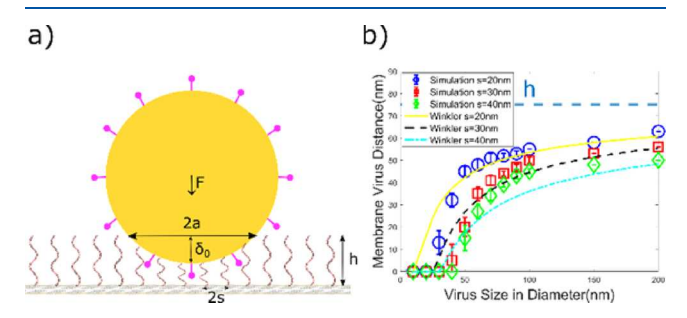


**Figure 5.** (a) Winkler foundation model to describe the surface response of an elastic solid. (b) Plot of indentation depth as a function of HS mesh and virus size in the case F = 20 pN: results of simulation and theory are in good agreement.

spike-like objects on the virion surface, these are typically much shorter than the glycocalyx thickness ( $\sim$ 10 nm for SARS-COV-2 vs hundreds of nm thick glycocalyx). Therefore, the primary resistance comes from the interaction of the virion body with the glycocalyx. Approximating the spherical indenter surface by a parabolic profile, the indentation at radial distance r is:

$$\delta = \delta_{\rm o} - \frac{r^2}{2R} \tag{5}$$

which is zero at r = a so

$$\delta_{\rm o} = \frac{a^2}{2R}; \ a^2 = 2R\delta_{\rm o} \tag{6}$$

The total force is

$$F = \int_{s}^{a} 2\pi r dr k \left( \delta_{o} - \frac{r^{2}}{2R} \right)$$

$$= 2\pi k \left[ (a^{2} - s^{2}) \frac{\delta_{o}}{2} - \frac{(a^{4} - s^{4})}{8R} \right]$$
(7)

It is evident that as  $a \to s$ ,  $F \to 0$ , i.e., there is no penetration resistance. Substituting in the relation between a and  $\delta$ , we get

$$F = \pi \frac{E}{h} \left[ R \delta_{\rm o}^2 - s^2 \delta_{\rm o} + \frac{s^4}{4R} \right] \tag{8}$$

Solving the above equation for  $\delta_0$ :

$$\delta_{\rm o} = \frac{s^2}{2R} + \sqrt{\frac{Fh}{\pi RE}} \tag{9}$$

To test the quality of this model, the indentation depth of viruses with different sizes and an applied force of 20 pN for three different HS spacing (2S = 20, 30, and 40 nm) were calculated using eq 9. A comparison with the simulation results is plotted in Figure 5b. The results show that the simulation data agree well with the model based on a Winkler foundation, especially in the cases where virus are large.

**Effect of Virus–HS Affinity.** Next, we wish to examine the third hypothesis that the virus can penetrate the glycocalyx without external force with the aid of weak but multivalent attraction to the HS.  $^{41,48}$  We added to our model host–cell receptors attached to the membrane plane. We chose a 1:1.5 ratio of HS to receptors because receptors are typically abundant throughout the surface.  $^{49}$  To assign the location of host cell receptors with no bias, the membrane area was divided into 625 (25 × 25) sub-areas, 50 of which were chosen at random to be populated by a receptor.

The indentation simulations discussed so far show that both small and larger viruses (compared with HS mesh size) can reach the membrane despite the glycocalyx layer under a sufficient externally applied force. However, we do not know if large viruses can pass the glycocalyx barrier without the aid of external force. Inspired by the recent findings that viruses can attach to HS on the cell surface, we hypothesize that the attraction underlying this attachment can aid in large virus penetration. We designed a simulation as described below and shown in Figure 6. Four large virus beads (D=80 nm) were situated initially at a distance of 15 nm above the top of the glycocalyx, and the overall system was in a unit box with

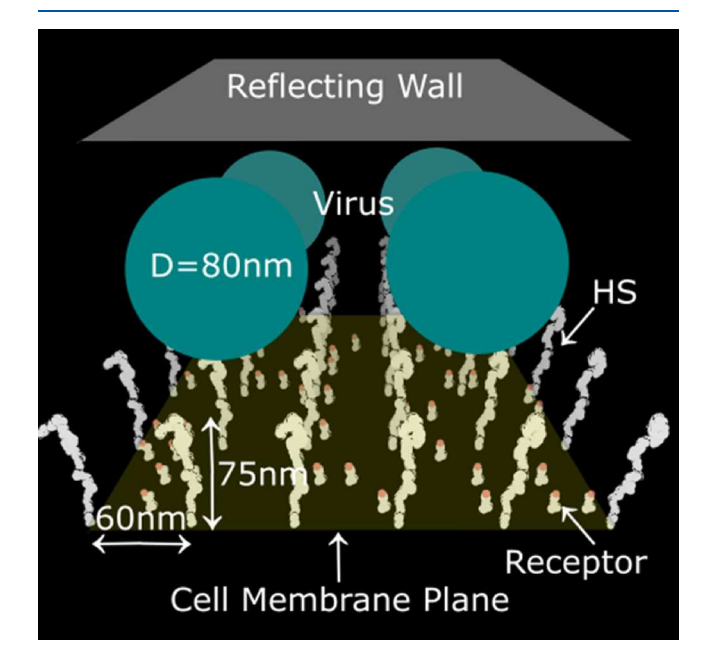


Figure 6. Coarse-grained model to represent viral particles interacting with the glycocalyx: (1) brush-like chains of HS beads, each with one end fixed in the cell membrane, (2) a collection of membrane-bound receptors represented by a string of MLD beads with one end frozen at the cell surface and the other end attached to a receptor bead that has attractive interaction with virus beads, and (3) four large green beads initially on top of HS chains representing typical virus particles. (4) Background repulsion force is assigned to the cell membrane surface, which forbids the penetration of any beads past the membrane plane. A reflecting wall at the top of the box confines viral particles to a relatively small volume above the glycocalyx.

dimensions: 360 nm  $\times$  360 nm  $\times$  200 nm. For the x and y directions, periodic boundary conditions were applied. For the z direction, a background repulsion force field was set at the bottom to prevent any beads in the system from passing through, resembling an impermeable cell membrane. To confine the virus, a LAMMPS fix wall/reflect function was applied at z=200 nm, the top of the box. Any beads that hit the surface at z=200 nm switched to the opposite direction with the same speed in the "z" direction, while retaining x- and y-direction movement unchanged.

The important parameter relevant to the hypothesis is the affinity between HS and virus beads. We studied the effect of HS-virus affinity by varying it from  $0.5K_BT$  to  $50K_BT$  while holding constant the HS density, cell receptor distribution, and virus size. We also conducted control simulations in which no HS chains exist in the system. Each case was repeated 5 times, and data from 20 simulated virus trajectories were collected.

Figure 7 shows four snapshots from a typical simulation for both the cases when HS-virus affinity  $(4K_BT)$  is on (Figure

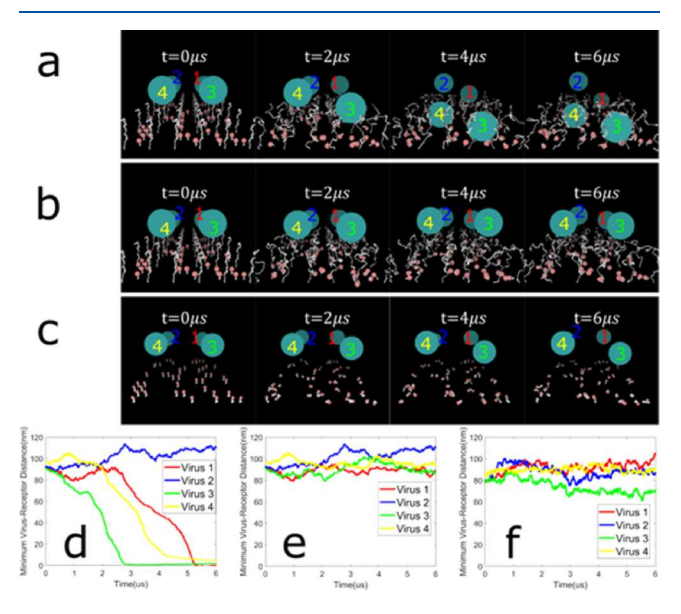


Figure 7. Snapshots from different stages of a typical simulation for HS-virus affinity "on", "off", and no-HS cases (a-c). Distance between each viral particle and its closest host cell receptor as a function of time for the affinity "on", "off", and no HS cases (d-f).

7a) and off (Figure 7b). Time t=0  $\mu$ s represents the initial state in which four virus beads were located 15 nm above the HS chains. At t=2  $\mu$ s, one of the virus particles in the affinity-on case had an initial attachment with HS chains and was pulled down slightly into the glycocalyx, while the other viruses continued to move around on top of the glycocalyx. At t=4  $\mu$ s, two of the viruses had been pulled onto the cell membrane. At t=6  $\mu$ s, three virus beads are situated adjacent to the cell surfaces, with one continuing to diffuse above the HS glycocalyx surface. In contrast, when HS-affinity was turned off, all four virus beads continued to move on top of the HS structure, repelled from and unable to penetrate it. Figure 7c shows a case in which the glycocalyx has been removed entirely. In this case too (Figure 7c), the viral beads fail to find the receptors within the duration of the simulation.

Figure 7d-f plots the smallest distance between each virus and all the host cell receptors throughout the simulation for the affinity on, off, and control cases (no HS). Three of four of

the viruses in the affinity-on cases reached the cell surface and were held onto it through the remainder of the simulation by the virus—receptor attraction (Figure 7d). For the cases where HS—virus affinity was turned off, none of the viruses managed to reach the cell membrane by the end of the simulation. They remained more than 70 nm away from the surface, meaning that the HS chains repelled the virus beads, preventing them from penetrating the glycocalyx (Figure 7e). Figure 7f shows that even when the glycocalyx is removed, the viral beads do not diffuse to find the receptors within the duration of the simulation. This indicates that the weak, multivalent interaction between the glycocalyx and viral particles can transport the latter more effectively than passive diffusion.

Figure 8 plots the binding ratio as a function of time for various affinity strengths. The binding ratio was calculated by

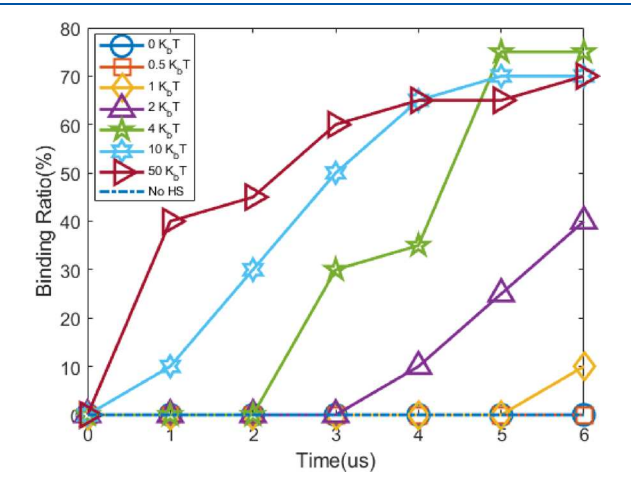


**Figure 8.** Plot of the binding ratio vs simulation time for varying HS-virus binding strength, and a control case in which the glycocalyx is removed ("No HS"). Stronger affinity increases the virus—receptor binding ratio and accelerates the binding events.

dividing the number of receptor-bound cases by the overall number of cases for that particular binding strength. The definition of binding is that the minimum virus—receptor surface distance reaches and stays close to zero, such as viruses 1, 3, and 4 in Figure 7a. These results show how stronger affinity results in quicker increase in the binding ratio. For the cases where HS does not exist, the viruses cannot find their binding partners within the simulation period.

**Engulfment Model.** We hypothesize that the weak multivalent attraction between the virus and glycocalyx drives engulfment, which is resisted by an elastic energy penalty. Let the reference state be of the virus particle outside the glycocalyx. If it is smaller than the typical distance between brush molecules in the glycocalyx, the virus will readily diffuse through to its receptor. However, if its size is larger than spacing, absent external forces, it can be engulfed by the glycocalyx, which suffers associated deformation. In order to better understand the conditions that favor engulfment, we propose a model in which free energy is reduced by adhesive interactions between the glycocalyx and the virus, and increased due to the attendant elastic deformation of the glycocalyx required to accommodate the virus (Figure 9).

Consider a spherical virus of radius A and let the gap between adjacent HS chains in the glycocalyx be 2a. If A > a, the glycocalyx network must be expanded to accommodate the virus. The total elastic energy  $(U_{ee})$  is calculated as

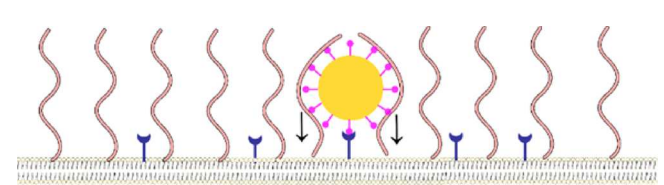


**Figure 9.** Model for the engulfment phenomenon, in which engulfment is driven by adhesive interactions and resisted by elastic forces.

follows,<sup>50–53</sup> based on a well-known solution for the pressure in expanding a spherical cavity in a neo-Hookean material:

$$P = \frac{E}{6} \left( 5 - \frac{4}{\lambda} - \frac{1}{\lambda^4} \right) \tag{10}$$

Here, P is the pressure, E is Young's modulus of the glycocalyx, and  $\lambda$  is the ratio of deformed and undeformed radii, R/a. The total elastic energy,  $U_{\rm ee}$ , can be calculated in increments:

$$dU_{ee} = PdV = P4\pi R^2 dR \tag{11}$$

By definition:

$$\lambda = \frac{R}{a}; \, \lambda^* = \frac{A}{a} \tag{12}$$

Therefore,

$$\lambda^2 = \frac{R^2}{a^2}; \, \mathrm{d}V = 4\pi\lambda^2 a^3 \mathrm{d}\lambda \tag{13}$$

Substituting this back into the expression for elastic energy:

$$U_{ee} = \int_{1}^{\lambda^{*}} P dV$$

$$= \frac{10}{9} \pi A^{3} E - \frac{4}{3} \pi a A^{2} E + \frac{2}{3} \frac{\pi a^{4} E}{A} - \frac{4}{9} \pi a^{3} E$$
(14)

For spontaneous engulfment, the elastic energy must be smaller than the adhesive energy:

$$\frac{10}{9}\pi A^{3}E - \frac{4}{3}\pi aA^{2}E + \frac{2}{3}\frac{\pi a^{4}E}{A} - \frac{4}{9}\pi a^{3}E < U_{ad}$$
 (15)

To determine the total adhesion energy, we calculated the distance D between each HS beads and virus at the last timestep of the simulation. We defined the binding to occur when D < 42 nm, which is slightly higher than the sum of radius of the HS bead and virus bead (40.5 nm) to ensure all the binding events are counted. Then, we calculate and sum the binding free energy for each binding event. For the case where the binding free energy is equal to  $2K_{\rm B}T$ , we found 626 binding cases, and the total adhesion energy was calculated as  $520.5K_{\rm B}T$ .

Then, eq 14 can be used to calculate  $U_{\rm ee}$  as:

$$U_{ee} = 53.7K_{\rm B}T\tag{16}$$

Showing that engulfment is indeed favored.

## CONCLUSIONS

Although the glycocalyx is nearly universally present on cell surfaces through which viruses infect cells, there is a little account in the literature of how viruses penetrate it. In this study, we examined some hypotheses for how viruses penetrate through the glycocalyx to adhere to their receptors on the cell membrane. We built a coarse-grained model for our system, including a brush-like glycocalyx, receptors, and viral particles. We conducted Brownian dynamics simulations to study penetration driven by an external force or weak multivalent adhesion between the glycocalyx and viral particles.

One possible mechanism we found from this study is that viruses can use their adhesive binding with the HS, the main component of the glycocalyx, to be engulfed by and transported through the glycocalyx to the cell surface. We hypothesize that this process is initialized by virus—HS attachment. The flexible HS structure makes it easy for viruses to touch more HS chains underneath them; in return, those chains generate additional driving force pulling the virus toward the membrane. Although the single HS—virus affinity is weak, the overall force accumulation makes it strong enough for the virus to be engulfed and to diffuse in the glycocalyx (Figure 10). We also found that once this HS—virus

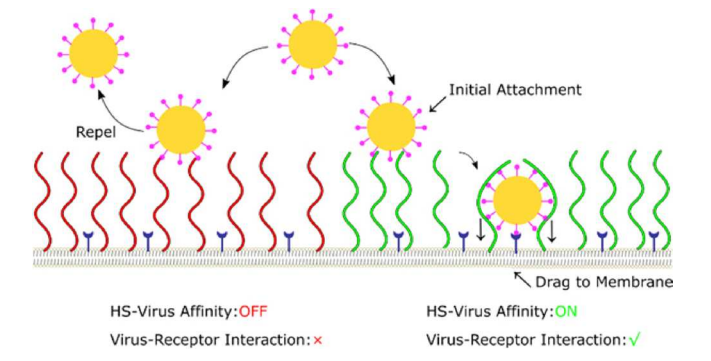


Figure 10. Hypothesis for HS acting as protection against virus penetration. The virus will be repelled by the steric hindrance and electrostatic repulsion force if HS—virus affinity does not exist or is not strong enough (HS in red). With sufficient affinity and following initial attachment, the brush will attract the virus and pull it toward the membrane. This process is favored if the decrease in free energy due to adhesion is greater than the increase in free energy due to elastic deformation needed to accommodate the viral particle.

interaction is shut down or made small enough, the glycocalyx structure will protect pathogen penetration through steric hindrance and electrostatic repulsion. We developed an analytical model for this process based on free energy reduction due to adhesion opposed by free energy increase due to elastic deformation required to accommodate the viral particle.

An example of the sort of adhesive interaction we postulate here is the experimental evidence for HS-virus affinity between S2 proteins on the SARS-CoV-2 virus and HS proteoglycans. Our results are consistent with several recent reports that the HS-virus attachment is crucial for virus infection. For example, the negative charges on HS can interact with the positive charge inside the S2 protein of the virus and therefore open its structure, exposing the RBD to host receptors. Our findings identify an additional mechanism: engulfment of the virus accommodated by elastic deformation of the glycocalyx.

Our results for force-driven virus penetration show that, unsurprisingly, viruses smaller than the spacing between molecules in the brush are readily pushed through the membrane plane. Viruses larger in size than the spacing can be pushed toward the membrane and reach a certain distance

depending on the maximum load and glycocalyx elasticity. We developed an analytical model based on contact mechanics of the virus on glycocalyx, represented by a Winkler foundation.

Our work has several limitations. First, our model is composed of beads representing the essential elements of the virus, receptor, and glycocalyx. However, the actual physiological system is far more sophisticated than a collection of beads. In addition, we have a simple brush-like structure of the glycocalyx. This should be examined in future work. Our research on HS-virus strength study assumes that all the monomers in HS have equal affinity. However, the glycocalyx is a heterogeneous structure such that some units can have stronger binding than others. Our virus is represented by a spherical bead, which assumes that the ligands on the virus surface are in high density. However, this varies from case to case, and a study on the effect of ligand density is helpful to get a more concrete conclusion. In our work, we have not accounted for the fact that the glycocalyx is attached to a fluidlike membrane and therefore its density fluctuates. Whether these fluctuations can be large enough to provide spontaneous access to virions is an interesting question for future study. The solvent is represented implicitly. This captures many of its effects but not others. Future exploration of factors, such as HS chain height, persistence length, and sequence, will be beneficial.

We have also assumed that the glycocalyx tethers on the cell membrane are not mobile over the time scale of the events modeled here. Relaxing this assumption would be an interesting future avenue for research.

Our focus in this work has been on the initial binding between a cell and a virion. This commonly provides the first step for infection. Subsequent events during infection vary depending on the particular virus and cell. For example, internalization is generally either by receptor-mediated endocytosis or by direct fusion with the cell membrane. Both mechanisms require large membrane deflections and are potentially mediated by the glycocalyx, but this is left for future development.

## ASSOCIATED CONTENT

## Supporting Information

The Supporting Information is available free of charge at https://pubs.acs.org/doi/10.1021/acs.jpcb.2c06662.

Single chain equilibrium test to validate the assumption that we are choosing conformations from an equilibrium ensemble and details on how Young's modulus of the glycocalyx is calculated using CG-MD simulation results (PDF)

# AUTHOR INFORMATION

## **Corresponding Author**

Anand Jagota — Department of Bioengineering and Department of Chemical and Biomolecular Engineering, Lehigh University, Bethlehem, Pennsylvania 18015, United States; orcid.org/0000-0002-0779-0880; Phone: 610 758 4396; Email: anj6@lehigh.edu

## **Authors**

Xinyu Cui — Department of Bioengineering, Lehigh University, Bethlehem, Pennsylvania 18015, United States

X. Frank Zhang – Department of Bioengineering, Lehigh University, Bethlehem, Pennsylvania 18015, United States; Present Address: Department of Biomedical Engineering, University of Massachusetts Amherst, Amherst, Massachusetts 01003, United States; orcid.org/0000-0002-8778-595X

Complete contact information is available at: https://pubs.acs.org/10.1021/acs.jpcb.2c06662

## **Author Contributions**

The manuscript was written through contributions of all authors. All authors have given approval to the final version of the manuscript.

#### **Notes**

The authors declare no competing financial interest.

## ACKNOWLEDGMENTS

This work was supported by NIH grants AI133634 and AI163708 and HL157975 and by NSF grant 1804117. The PIs would also like to acknowledge partial support for this work from NSF grant 2200066: "PIPP Phase I: Dynamics of Pandemic Spread and Prevention in Indigenous Communities".

## REFERENCES

- (1) Lefebvre, A.; Fiet, C.; Belpois-Duchamp, C.; Tiv, M.; Astruc, K.; Aho Glele, L. S. Case fatality rates of Ebola virus diseases: a meta-analysis of World Health Organization data. *Med. Mal. Infect.* **2014**, 44, 412–416.
- (2) Dixon, M. G.; Schafer, I. J.; Centers for Disease Control and Prevention (CDC). Ebola viral disease outbreak-West Africa, 2014. *MMWR Morb. Mortal. Wkly Rep.* **2014**, *63*, 548–551.
- (3) Mbonye, A. K.; Wamala, J. F.; Nanyunja, M.; Opio, A.; Makumbi, I.; Aceng, J. R. Ebola viral hemorrhagic disease outbreak in West Africa- lessons from Uganda. *Afr. Health Sci.* **2014**, *14*, 495–501.
- (4) de Groot, R. J.; Baker, S. C.; Baric, R. S.; Brown, C. S.; Drosten, C.; Enjuanes, L.; Fouchier, R. A.; Galiano, M.; Gorbalenya, A. E.; Memish, Z. A.; Perlman, S.; Poon, L. L. M.; Snijder, E. J.; Stephens, G. M.; Woo, P. C. Y.; Zaki, A. M.; Zambon, M.; Ziebuhr, J. Middle East respiratory syndrome coronavirus (MERS-CoV): announcement of the Coronavirus Study Group. *J. Virol.* 2013, 87, 7790–7792.
- (5) Zaki, A. M.; van Boheemen, S.; Bestebroer, T. M.; Osterhaus, A. D.; Fouchier, R. A. Isolation of a novel coronavirus from a man with pneumonia in Saudi Arabia. *N. Engl. J. Med.* **2012**, *367*, 1814–1820.
- (6) Memish, Z. A.; Zumla, A. I.; Al-Hakeem, R. F.; Al-Rabeeah, A. A.; Stephens, G. M. Family cluster of Middle East respiratory syndrome coronavirus infections. *N. Engl. J. Med.* **2013**, 368, 2487–2494
- (7) Bar-On, Y. M.; Flamholz, A.; Phillips, R.; Milo, R. SARS-CoV-2 (COVID-19) by the numbers. *eLife* **2020**, *9*, No. e57309.
- (8) Pedersen, S. F.; Ho, Y.-C. SARS-CoV-2: a storm is raging. *J. Clin. Invest.* **2020**, 130, 2202–2205.
- (9) Li, Q.; Guan, X.; Wu, P.; Wang, X.; Zhou, L.; Tong, Y.; Ren, R.; Leung, K. S. M.; Lau, E. H. Y.; Wong, J. Y.; et al. Early Transmission Dynamics in Wuhan, China, of Novel Coronavirus-Infected Pneumonia. N. Engl. J. Med. 2020, 382, 1199–1207.
- (10) Huang, C.; Wang, Y.; Li, X.; Ren, L.; Zhao, J.; Hu, Y.; Zhang, L.; Fan, G.; Xu, J.; Gu, X.; et al. Clinical features of patients infected with 2019 novel coronavirus in Wuhan, China. *Lancet* **2020**, 395, 497–506.
- (11) Li, F. Structure, Function, and Evolution of Coronavirus Spike Proteins. *Annu. Rev. Virol.* **2016**, *3*, 237–261.
- (12) Perlman, S.; Netland, J. Coronaviruses post-SARS: update on replication and pathogenesis. *Nat. Rev. Microbiol.* **2009**, *7*, 439–450. (13) Cohen, F. S. How Viruses Invade Cells. *Biophys. J.* **2016**, *110*,

1028-1032.

- (14) Mockl, L. The Emerging Role of the Mammalian Glycocalyx in Functional Membrane Organization and Immune System Regulation. *Front. Cell Dev. Biol.* **2020**, *8*, 253.
- (15) Weinbaum, S.; Tarbell, J. M.; Damiano, E. R. The structure and function of the endothelial glycocalyx layer. *Annu. Rev. Biomed. Eng.* **2007**, *9*, 121–167.
- (16) Reitsma, S.; Slaaf, D. W.; Vink, H.; van Zandvoort, M. A.; oude Egbrink, M. G. The endothelial glycocalyx: composition, functions, and visualization. *Pflugers Arch.* **2007**, *454*, 345–359.
- (17) Cui, X.; Lapinski, N.; Zhang, X. F.; Jagota, A. Length of mucin-like domains enhances cell-Ebola virus adhesion by increasing binding probability. *Biophys. J.* **2021**, *120*, 781–790.
- (18) Ihrcke, N. S.; Wrenshall, L. E.; Lindman, B. J.; Platt, J. L. Role of heparan sulfate in immune system-blood vessel interactions. *Immunol. Today* **1993**, *14*, 500–505.
- (19) Pries, A. R.; Secomb, T. W.; Gaehtgens, P. The endothelial surface layer. *Pflugers Arch.* **2000**, 440, 653-666.
- (20) Camejo, G.; Hurt-Camejo, E.; Wiklund, O.; Bondjers, G. Association of apo B lipoproteins with arterial proteoglycans: pathological significance and molecular basis. *Atherosclerosis* 1998, 139, 205–222.
- (21) Seog, J.; Dean, D.; Rolauffs, B.; Wu, T.; Genzer, J.; Plaas, A. H.; Grodzinsky, A. J.; Ortiz, C. Nanomechanics of opposing glycosaminoglycan macromolecules. *J. Biomech.* **2005**, *38*, 1789–1797.
- (22) van den Berg, B. M.; Nieuwdorp, M.; Stroes, E. S.; Vink, H. Glycocalyx and endothelial (dys) function: from mice to men. *Pharmacol. Rep.* **2006**, *58*, 75–80.
- (23) Delgadillo, L. F.; Marsh, G. A.; Waugh, R. E. Endothelial Glycocalyx Layer Properties and Its Ability to Limit Leukocyte Adhesion. *Biophys. J.* **2020**, *118*, 1564–1575.
- (24) Targosz-Korecka, M.; Jaglarz, M.; Malek-Zietek, K. E.; Gregorius, A.; Zakrzewska, A.; Sitek, B.; Rajfur, Z.; Chlopicki, S.; Szymonski, M. AFM-based detection of glycocalyx degradation and endothelial stiffening in the db/db mouse model of diabetes. *Sci. Rep.* **2017**, *7*, 15951.
- (25) Clifford, C. A.; Seah, M. P. Nanoindentation measurement of Young's modulus for compliant layers on stiffer substrates including the effect of Poisson's ratios. *Nanotechnology* **2009**, *20*, No. 145708.
- (26) Clifford, C. A.; Seah, M. Modelling of nanomechanical nanoindentation measurements using an AFM or nanoindenter for compliant layers on stiffer substrates. *Nanotechnology* **2006**, *17*, 5283.
- (27) Butt, H.-J.; Kappl, M.; Mueller, H.; Raiteri, R.; Meyer, W.; Rühe, J. Steric forces measured with the atomic force microscope at various temperatures. *Langmuir* 1999, 15, 2559–2565.
- (28) Hertz, H. On the contact of elastic solids. Z. Reine Angew. Math. 1882, 92, 156–171.
- (29) Jiang, X. Z.; Feng, M.; Luo, K. H.; Ventikos, Y. Large-scale molecular dynamics simulation of flow under complex structure of endothelial glycocalyx. *Comput. Fluids* **2018**, *173*, 140–146.
- (30) Cruz-Chu, E. R.; Malafeev, A.; Pajarskas, T.; Pivkin, I. V.; Koumoutsakos, P. Structure and Response to Flow of the Glycocalyx Layer. *Biophys. J.* **2014**, *106*, 232–243.
- (31) Shriver, Z.; Capila, I.; Venkataraman, G.; Sasisekharan, R. Heparin and heparan sulfate: analyzing structure and microheterogeneity. *Handb. Exp. Pharmacol.* **2012**, 207, 159–176.
- (32) Kroon-Batenburg, L. M.; Kruiskamp, P. H.; Vliegenthart, J. F.; Kroon, J. Estimation of the persistence length of polymers by MD simulations on small fragments in solution. Application to cellulose. *J. Phys. Chem. B* **1997**, *101*, 8454–8459.
- (33) Flory, P. J.; Volkenstein, M. Statistical mechanics of chain molecules; Wiley Online Library, 1969.
- (34) German Advisory Committee Blood (Arbeitskreis Blut), Subgroup 'Assessment of Pathogens Transmissible by Blood'. Human Immunodeficiency Virus (HIV). *Transfus. Med. Hemother.* **2016**. *43*, 203–222.
- (35) Kramer, J. R.; Onoa, B.; Bustamante, C.; Bertozzi, C. R. Chemically tunable mucin chimeras assembled on living cells. *Proc. Natl. Acad. Sci. U. S. A.* **2015**, *112*, 12574–12579.

- (36) Santiago, C.; Ballesteros, A.; Martinez-Munoz, L.; Mellado, M.; Kaplan, G. G.; Freeman, G. J.; Casasnovas, J. M. Structures of T cell immunoglobulin mucin protein 4 show a metal-Ion-dependent ligand binding site where phosphatidylserine binds. *Immunity* **2007**, *27*, 941–951.
- (37) Yan, R.; Zhang, Y.; Li, Y.; Xia, L.; Guo, Y.; Zhou, Q. Structural basis for the recognition of SARS-CoV-2 by full-length human ACE2. *Science* **2020**, *367*, 1444–1448.
- (38) Thompson, A. P.; Aktulga, H. M.; Berger, R.; Bolintineanu, D. S.; Brown, W. M.; Crozier, P. S.; in 't Veld, P. J.; Kohlmeyer, A.; Moore, S. G.; Nguyen, T. D.; et al. LAMMPS a flexible simulation tool for particle-based materials modeling at the atomic, meso, and continuum scales. *Comput. Phys. Commun.* **2022**, 271, No. 108171.
- (39) Zhang, Q.; Tian, F.; Wang, F.; Guo, Z.; Cai, M.; Xu, H.; Wang, H.; Yang, G.; Shi, X.; Shan, Y.; et al. Entry Dynamics of Single Ebola Virus Revealed by Force Tracing. ACS Nano 2020, 14, 7046–7054.
- (40) Dragovich, M. A.; Fortoul, N.; Jagota, A.; Zhang, W.; Schutt, K.; Xu, Y.; Sanabria, M.; Moyer, D. M., Jr.; Moller-Tank, S.; Maury, W.; et al. Biomechanical characterization of TIM protein-mediated Ebola virus-host cell adhesion. *Sci. Rep.* **2019**, *9*, 267.
- (41) Liu, L.; Chopra, P.; Li, X.; Bouwman, K. M.; Tompkins, S. M.; Wolfert, M. A.; de Vries, R. P.; Boons, G.-J. Heparan Sulfate Proteoglycans as Attachment Factor for SARS-CoV-2. *ACS Cent. Sci.* **2021**, *7*, 1009–1018.
- (42) Wojczynski, M. K.; Glasser, S. P.; Oberman, A.; Kabagambe, E. K.; Hopkins, P. N.; Tsai, M. Y.; Straka, R. J.; Ordovas, J. M.; Arnett, D. K. High-fat meal effect on LDL, HDL, and VLDL particle size and number in the Genetics of Lipid-Lowering Drugs and Diet Network (GOLDN): an interventional study. *Lipids Health Dis.* **2011**, *10*, 181.
- (43) Humphrey, W.; Dalke, A.; Schulten, K. VMD: visual molecular dynamics. J. Mol. Graph. 1996, 14, 33–38.
- (44) Weinbaum, S.; Zhang, X.; Han, Y.; Vink, H.; Cowin, S. C. Mechanotransduction and flow across the endothelial glycocalyx. *Proc. Natl. Acad. Sci. U. S. A.* **2003**, *100*, 7988–7995.
- (45) Johnson, K. L. Contact Mechanics; Cambridge University Press, 1985.
- (46) Mansfield, E. H. The bending and stretching of plates; 2009.
- (47) Dillard, D. A.; Mukherjee, B.; Karnal, P.; Batra, R. C.; Frechette, J. A review of Winkler's foundation and its profound influence on adhesion and soft matter applications. *Soft Matter* **2018**, 14, 3669–3683.
- (48) Wang, Q.; Zhang, Y.; Wu, L.; Niu, S.; Song, C.; Zhang, Z.; Lu, G.; Qiao, C.; Hu, Y.; Yuen, K.-Y.; et al. Structural and Functional Basis of SARS-CoV-2 Entry by Using Human ACE2. *Cell* **2020**, *181*, 894–904.
- (49) Hamming, I.; Timens, W.; Bulthuis, M. L.; Lely, A. T.; Navis, G.; van Goor, H. Tissue distribution of ACE2 protein, the functional receptor for SARS coronavirus. A first step in understanding SARS pathogenesis. *J. Pathol.* **2004**, *203*, 631–637.
- (50) Green, A. E.; Zerna, W. Theoretical elasticity; Courier Corporation, 1992.
- (51) Gent, A.; Lindley, P. Internal rupture of bonded rubber cylinders in tension. *Proc. R. Soc. London, Ser. A* **1959**, 249, 195–205.
- (52) Gent, A.; Tompkins, D. Surface energy effects for small holes or particles in elastomers. *J. Polym. Sci., Polym. Phys. Ed.* **1969**, *7*, 1483–1487.
- (53) Dollhofer, J.; Chiche, A.; Muralidharan, V.; Creton, C.; Hui, C. Surface energy effects for cavity growth and nucleation in an incompressible neo-Hookean material—modeling and experiment. *Int. J. Solids Struct.* **2004**, *41*, 6111–6127.
- (54) Clausen, T. M.; Sandoval, D. R.; Spliid, C. B.; Pihl, J.; Perrett, H. R.; Painter, C. D.; Narayanan, A.; Majowicz, S. A.; Kwong, E. M.; McVicar, R. N.; et al. SARS-CoV-2 Infection Depends on Cellular Heparan Sulfate and ACE2. *Cell* **2020**, *183*, 1043–1057.